Short Communication

Study on the Characteristics of MAO/Polymer/Ni Three-Layer Composite Film formed on AZ31 Magnesium Alloy

Hung-Bin Lee[1], Hung-Hua Sheu[2, 3], Jia-Sian, Jian[1], Ruey-Chang Hsiao[4,*

[1] Department of Optoelectronics and Materials Technology & Center of Excellence for Ocean Engineering, National Taiwan Ocean University, Keelung 202, Taiwan, ROC.
[2] Department of Chemical & Materials Engineering, Chung Cheng Institute of Technology, National Defense University, Dasi, Taoyuan 335, Taiwan, ROC.
[3] System Engineering and Technology Program, National Yang Ming Chiao Tung University, Hsin-Chu, 300, Taiwan, ROC.
[4] Department of Chemical and Materials Engineering, Lunghwa University of Science and Technology, Taoyuan334, Taiwan, ROC.
[*]E-mail: hrc@gm.lhu.edu.tw

In this study, MAO/Polymer/Ni three-layer composite coating deposited on AZ 31 magnesium alloy was carried out by micro-arc oxidation, spinning coated and eletroless Ni processes. The characteristics of different coatings were analyzed by XRD, SEM, TEM and EDS. The MAO film subsequent sealing with polymer layer, the polymer agent will fill up the micro-arc holes of MAO film. Finally, an electroless nickel layer were deposited on polymer film to form a MAO/polymer/Ni composite coating. It can significantly decrease the i_{corr} value from 39.6×10^{-6} A/cm^2 to 7.2×10^{-6} A/cm^2. The MAO/polymer/Ni coating significantly enhanced the corrosion resistance of the AZ31alloy due to the protection performance both of polymer and nickel layer.

1. INTRODUCTION

In recent years, due to the requirements of scientific and technological development, the lightweight and reuse of devices has gradually been valued by the industry. The common lightweight metals are mainly magnesium, aluminum, and titanium, among them, magnesium and its alloys have the lowest density (1.7g/cm³), have been extensively applied in industrial fields such as transportation, electronics, aerospace industry, and biomedical science due to their low density, low melting point, high

plasticity, good machinability, and biocompatibility [1,2]. However, magnesium alloys have poor corrosion resistance, which limits the application of magnesium alloys. In order to improve the corrosion resistance of magnesium alloys, many surface treatment technologies have been developed including physical vapor deposition, chemical vapor deposition, chemical conversion, micro-arc oxidation, electroplating, and electroless plating [3,4].

Micro-arc oxidation (MAO) is a kind of electrochemical process, which is mainly to put the test piece in the electrolyte, and form a ceramic oxide film layer on the surface of the test piece under the reaction of thermochemistry and plasma chemistry. This method can improve the corrosion resistance and wear resistance of samples. Yao et al. [5,6] presented that the use of pulsed power supply and discharge circuit to stabilize the micro-arc oxidation process and generate uniform arc points, thereby improving the microstructure and corrosion resistance of the MAO layer. Kamal et al. [7] reported that micro-arc oxidation parameters such as current density, electrode distance and oxidation time, etc., can be adjusted to obtain the MAO layer with the smallest porosity and increase the hardness of the layer. The electrolyte, oxidation time and temperature conditions used in micro-arc oxidation will affect the performance of coating [8-10]. In addition, the micro-arc oxidation parameters such as voltage, current, duty cycle, frequency, etc. have a great influence on the formation of cermet coatings [11-13]. Narayanan et al. [14] indicated that the MAO layer will be formed on the surface of the magnesium alloy after micro-arc oxidation, which can improve the corrosion resistance and the biocompatibility of the magnesium alloy. Krishna et al. [15] presented that the addition of aluminum and zinc to the magnesium alloy substrate can increase the reaction rate of the micro-arc oxide film layer. It can be found that the corrosion resistance is significantly increased by adding 3 wt% of aluminum to the magnesium/aluminum/zinc. Adding 5-9 wt% of aluminum can increase the microhardness, and zinc can increase the oxidation efficiency of aluminum and magnesium during micro-arc oxidation, and can increase the hardness, which can improve the corrosion resistance of magnesium alloys. The current supply methods of the micro-arc oxidation process are divided into the following types, direct current (DC), unipolar pulse current (PC), and bipolar pulse current (BPC) [16-18]. Srinivasan et al. [19] indicated that using the method of adjusting the current density to carry out the micro-arc oxidation, it is found that the MAO film formed when using a low current has a denser bond with the substrate and better adhesion. The MAO film formed under high current has larger holes and more microcracks, while reducing the adhesion of the MAO film to the substrate, the MAO film formed by high current is thicker and also has a higher roughness, but the surface has many holes and microcracks will lead to poor corrosion resistance. Owing to the AMO layer will have many holes and cracks after the micro-arc oxidation, the corrosive liquid will penetrate and it will weaken the protection of the AMO layer from the substrate. Therefore, coating a polymer layer on the AMO layer will improve the corrosion resistance of the coating. Zahidah et al. [20,21] indicated that adding corrosion inhibitors combined with related coatings can enhance the protection of the substrate metal. Li et al. [22] reported that coating a layer of organic-inorganic compound film on the MAO layer can improve the corrosion resistance of the test piece. After the test piece is immersed in a 3.5 wt% NaCl solution, the corrosion resistance of the test piece is significantly improved ($i_{corr} = 5.764 \times 10^{-9}$ A / cm^2), and this can be attributed to the joint contribution of hydrophobic film and MAO film in improving corrosion resistance. Li et al. [23] also indicated that using the method of combining resist and hydrophobic film layer, coat the corrosion-

resistant composite layer on the magnesium alloy samples to cover the holes on the surface of the micro-arc oxidation film, and then apply a hydrophobic wax film on the surface of the samples to improve corrosion resistance.

The technology of coating electroless nickel and nickel-phosphorus alloy coatings on the polymer film is an advanced metal surface protection technology developed in recent years. This technology can be applied in machinery, automobile and aerospace fields. Generally, the nickel-phosphorus alloy coatings has an excellent high hardness, wear resistance and corrosion resistance when the phosphorus content exceed 8 wt%. Using electroplating, electroless electroplating or composite electroplating process to form nickel-phosphorus alloy on the surface of the matrix material from the corrosive medium to achieve the function of protective coating. Gholizadeh et al. [24-26] indicated that adding WO_3 nano-particles into the Ni-based electroless bath, the microhardness and wear resistance of electroless Ni-based composite coating will be improved. Chen et al. [27] indicated that the electroless Ni coating has some excellent properties such as high corrosion resistance, high wear resistance, more uniform deposition, good electrical conductivity and good thermal conductivity. Previous literatures presented that the coatings has a better adhesion on substrates when the coatings has an amorphous structure [28,29]. Due to the potential difference between the electroless nickel plating and the magnesium alloy sample, the electroless nickel plating combined with the magnesium alloy sample is easily to electrochemical corrosion [30,31]. The other literatures indicated that when micro-arc oxidation is used as the intermediate layer, the electrochemical corrosion behavior between the magnesium alloy and the electroless nickel plating will be suppressed [32,33]. Lin et al. [34] indicated that When the phosphorus content of the electroplated nickel-phosphorus coating is about 6~14wt%, the coating will not show a passivation zone in the polarization curve. Lu et al. [35] presented that the addition of tungsten to the Ni-P alloy coating slightly improves the corrosion resistance of the coating, but the addition of molybdenum does not seem to have a significant effect on improving the corrosion resistance of the coating.

In this study, micro-arc oxidation technology is selected as the surface treatment process of magnesium alloy, after the preparation of the MAO film, the MAO film will be coated with a polymer layer, and finally electroless nickel plating will be coated on the polymer film layer. The prepared composite coating with three-layer structure was observed by TEM to investigate the sealing effect of the micro-arc oxidation layer caused by polymer layer and Ni-P coating and its influence on the corrosion resistance.

2. EXPERIMENTAL PROCEDURE

2.1. Preparation of the MAO composite coatings

AZ31 Mg alloy plate was cut into a dimension of 30 mm (L)×30 mm (W)×4 mm (T). They were ground with SiC paper up to 2000 grits, ultrasonically cleaned in ethanol for 3 minutes. The MAO process was performed using a pulsed bi-polar power source, a beaker with 2 L capacity, and a stainless-steel condenser as the electrolyte cell and cooling system, respectively. The electrolyte was prepared

using 6 g/L Na_2SiO_3, 5 g/L NaOH and 3 g/L NaF in DI water. The micro-arc oxidation reaction is carried out using a constant voltage method, and the operating conditions including the temperature, duty cycle, and voltage were set to 5°C, 30 %, and 260-300 V, respectively, the MAO processing time is 7 min.

The prepared MAO samples were ultrasonically cleaned in DI water and dried in a stream of warm air, then the M-bond 610 adhesive (two-component, solvent-thinned, epoxy-phenolic adhesive, solids content 22%, belongs to a commercial professional adhesive) was evenly applied to the MAO samples, and samples were placed on the heating plate at 100°C and baked for 30 minutes. After drying, place the MAO samples on the stage of the spin coater (MIKASA, MB-100), and evenly spread the blended agent on the surface of the MAO samples. Then start the spin coater. After coating, placed the samples on the heating plate at 100° C and bake for 30 minutes to dry the solvent. After cooling down, the samples were ultrasonically cleaned in DI water and dried in a stream of warm air, and finished the preparation of the polymer film.

The chemical nickel plating agent for this experiment was supplied by the Xiang-Shu Co., Ltd., Taiwan. The composition of electroless nickel plating agent was the NIE-282 B 15 wt% and NIE-282 A 6 wt% added into 1 L distilled water. The pH value of electroless nickel plating agent was 4.4-4.7, the plating temperature was at 86-95 °C. Firstly, the MAO test piece coated with polymer film was immersed in the prepreg slot CUB-2054, and the surface deoxidation reaction time was 2~4 min to enhance the activation and composition of palladium, then soaked the samples in the catalytic tank CUB-2055, the reaction time was 4~6 min to activate the palladium and generated Pd on the samples, finally soaked the samples in the electroless nickel plating agent to form Ni film.

2.2. Characterization

The morphology and microstructure of the MAO/Polymer/Ni three-layer composite coatings were observed via field-emission scanning electron microscopy (Hitachi FESEM S-4800) and transmission electron microscope (TEM, JEOL JEM-2100F). The chemical composition of three-layer composite coatings were confirmed using an energy dispersive spectrometer (EDS). The crystal structure of the samples was determined using an X-ray diffractometer (XRD, BRUKER D8 SSS).

Contact angle test of various samples were carried out with a water drop contact angle tester (Phoenix smart M), the samples including AZ31 magnesium alloy, MAO coatings, polymer coatings and MAO/Polymer/Ni three-layer composite coatings. The water drop type including DI water and 3.5 wt% NaClsolution.

The adhesion property of MAO coatings and MAO/Polymer/Ni three-layer composite coatings were carried out with a scratch tester (Scratch Tester, RST³). The load was from 0 N to 100 N, and the load was gradually applied to the test samples to measure the critical load that the MAO coatings and MAO/Polymer/Ni three-layer composite coatings.

The potentiodynamic polarization of MAO coatings and MAO/Polymer/Ni three-layer composite coatings were analyzed by an electrochemical measurement with a potentiostat (Zahner Zennium-E 41100) in a three electrode system comprising a platinum plate as counter electrode, a saturated calomel electrode (SCE) as reference electrode. The potentiodynamic polarization analysis

were conducted in 3.5 wt.% NaCl solution at room temperature. The polarization curve was then obtained by scanning from -3.0 to 0 V at a scanning rate of 1 mV/s. The anticorrosion ability was evaluated by electrochemical measurement with a potentiostat (Zahner-Elektrik GMBH & Co., Germany) in a three electrode system comprising a platinum plate as counter electrode, a saturated calomel electrode (SCE) as reference electrode. Due to the polymer film is not conductive, it is not included in the comparison of the corrosion polarization curves.

3. RESULTS AND DISCUSSION

3.1. Coating characterization
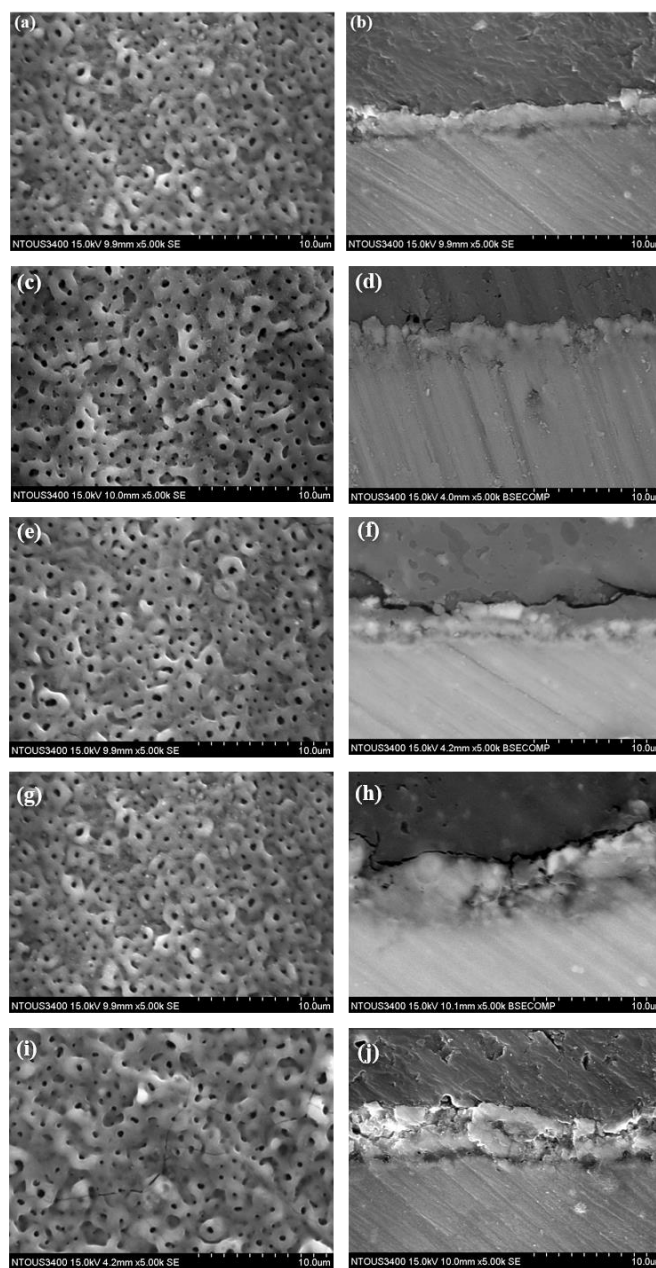
Figure 1. The SEM images of MAO coatings prepared from different voltage (a)(b) 260V, (c)(d) 270V, (e)(f) 280V, (g)(h) 290V, (i)(j) 300V.

Fig. 1 shows the SEM morphology and cross-sectional images of the MAO coatings used a pulsed bi-polar power source and carried out with different constant voltage from 260 V to 300 V.

It is found that there are many micropores on the surface of the MAO layer caused by the arc reaction in the micro-arc process, and these micropores are of different sizes. At the same time, micro-cracks caused by the rapid condensation of the oxide layer can also be found. These micro-cracks are formed due to the thermal stress caused by the rapid solidification of the film in the molten state [17]. The thickness of the MAO layer is about 2.42 μm after 7 minutes of micro-arc oxidation at a voltage of 260 V (Fig. 1.b). At the same micro-arc oxidation period (7 minutes), the thickness of the MAO layer formed at the voltage of 270, 280, 290 and 300 V is approximately at 3.11, 4.53, 5.11 and 4.11 um, respectively (Fig. 1d, f, h, j). It can be seen that the cross-section of the MAO film formed under the voltage of 290 V has begun to crack (Fig. 1h), and when the voltage rises to 300 V, the thickness of the MAO film drops to 4.4 μm and obvious cracks and peeling can be observed (Fig. 1j). The thickness of MAO films increase from 2.42 μm to 5.11 μm with the increment of operated voltage from 270 V to 290 V, but the MAO film began to crack at 290 V. The thickness of the MAO film drops to 4.4 μm at 300 V can be attributed to the excessive operated voltage will cause the micro-arc electric shock to break the formed MAO film and cause the MAO film to peel off, resulting in a decrease in the thickness of the MAO film. Therefore, in this study, 280 V is the optimal operated voltage for the formation of MAO film. SEM-EDS chemical composition analysis of MAO coatings presents that the highest fluorine content of MAO film occurred at 300 V (Table 1).

Table 1. The SEM-EDS chemical composition analysis of MAO coatings prepared using different operated voltage

Elements (at.%) / Voltage	Mg	F	Si	Al	O	Total
260 V	35.48	13.88	4.55	1.89	44.21	100.00
270 V	32.28	14.01	4.27	2.02	47.42	100.00
280 V	34.78	13.43	4.25	1.91	45.63	100.00
290 V	39.96	13.15	4.04	2.64	40.21	100.00
300 V	34.50	16.25	5.35	1.96	41.94	100.00

Fig. 2 shows the TEM cross-sectional image and SEM-EDS mapping line scanning, the image indicates that the dense layer of MAO film is near AZ31 magnesium alloy and the porous layer is near the surface of MAO film. The pore size of the porous layer ranges from a few microns to nanometers. Because some oxides are melted and condensed during the micro-arc oxidation reaction, and sufficient

energy and time are provided to promote the nucleation and growth of crystal grains, so the porous layer will have some relatively coarse grains, and most of them are mainly MgO. According to the analysis of TEM-EDS in the position a, b, c and d of the MAO film (Fig. 2a), fluorine is mostly deposited on the bottom layer of MAO film (Table 2), this phenomenon is agreement with the previous study [22].
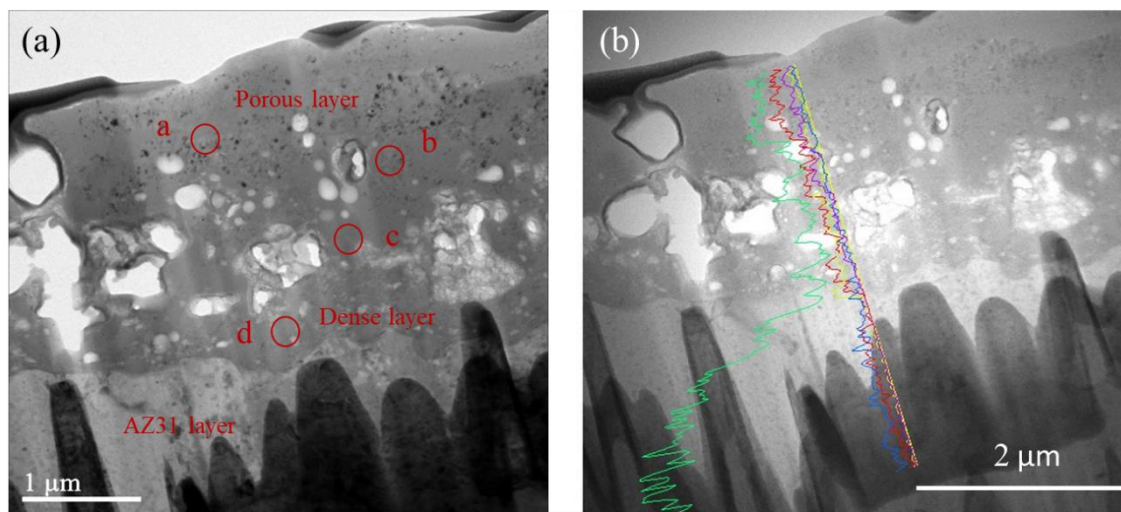

Figure 2. The TEM cross-sectional images of MAO coatings: (a) microstructure and analysis of EDS, (b) line scanning.

Table 2. The TEM-EDS chemical composition analysis of MAO coatings

Elements (at.%) Position	Mg	F	Si	Al	O	Total
a	31.86	10.82	6.24	1.23	49.89	100.00
b	35.25	11.34	5.18	1.44	46.80	100.00
c	31.85	16.98	6.36	1.04	43.77	100.00
d	31.96	18.42	2.56	2.08	44.97	100.00

When the polymer layer has not been coated on the MAO film, the MAO film has many holes and the holes are relatively large. Next, coat the polymer layer on the MAO layer, ultrasonic vibration allows the polymer agent to penetrate deeper into the MAO layer, then use a spin coater to disperse the polymer agent evenly in MAO film. Fig. 3b shows the thickness of polymer layer is approximately at 24.8 um without using a spin coater. When the rotation speed of the spin coater is 500 rpm, the polymer film thickness after 15 minutes of rotation is about 9 μm (Fig. 3c), the rotation speed of the spin coater increase to 750 rpm, the polymer film thickness is about 2-4 μm. Fig. 3 a presents that the original micro-arc holes of MAO film have been completely covered by the polymer layer, which means that the sealing process has been completed. The chemical composition of the layer analyzed by energy dispersive

spectrometer (EDS) all present carbon element, indicating this layer is polymer. Then electroless Ni layer on the surface of the polymer layer, to finish a MAO/polymer/Ni three layers composite coatings. In Fig. 4 and Fig. 5(a), both images show that the thickness of Ni film is approximately at 1.2 um.
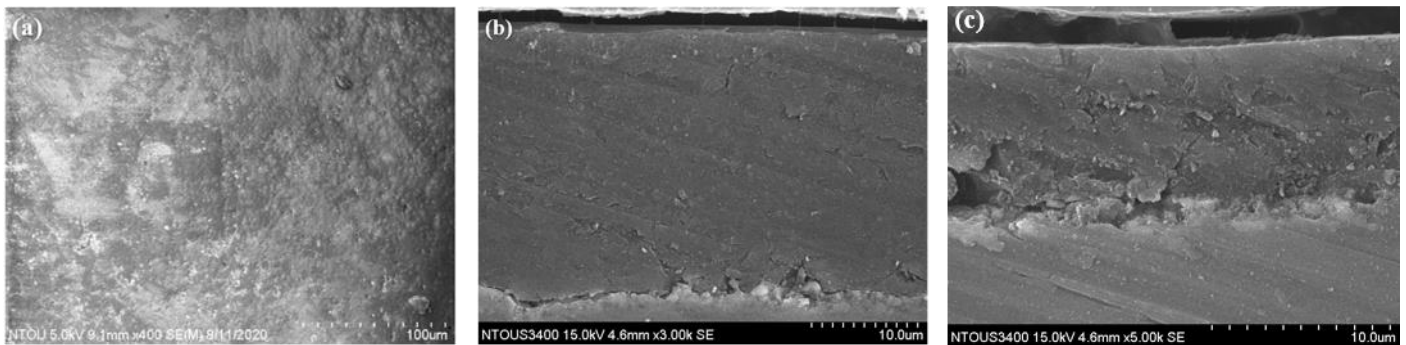

Figure 3. The SEM images of polymer layer: (a) surface morphology, (b) cross-sectional of un-spinned coated polymer layer, (c) cross-sectional of spinned coated polymer layer.
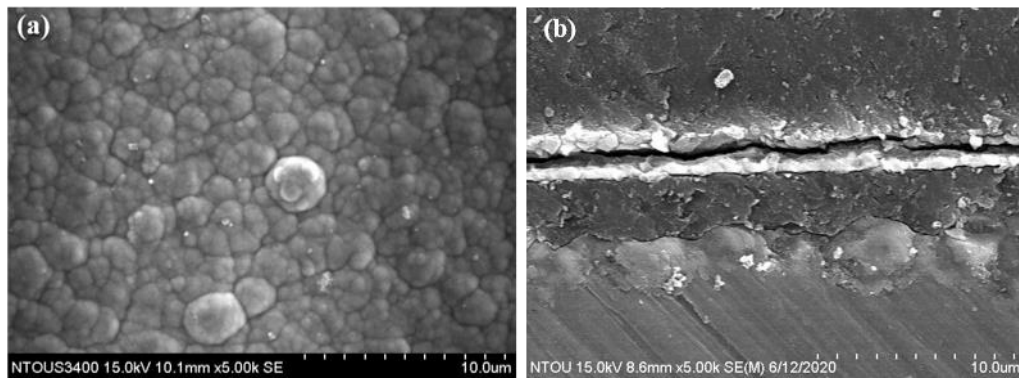

Figure 4. The SEM images of Ni film: (a) surface morphology (b) cross-sectional.

Table 3. The TEM-EDS analysis of MAO/polymer/Ni three layers coatings

Elements (at.%) / Specimens	Mg	F	Si	Al	O	C	Ni	P	Total
AZ31	93.55	0	0	1.31	5.14	0	0	0	100.00
MAO	29.39	6.43	3.23	0.62	51.83	3.01	0	4.84	100.00
Polymer	0	0	0	0	10.36	89.64	0	0	100.00
Ni	0	0	0	0	0	0	84.55	15.45	100.00
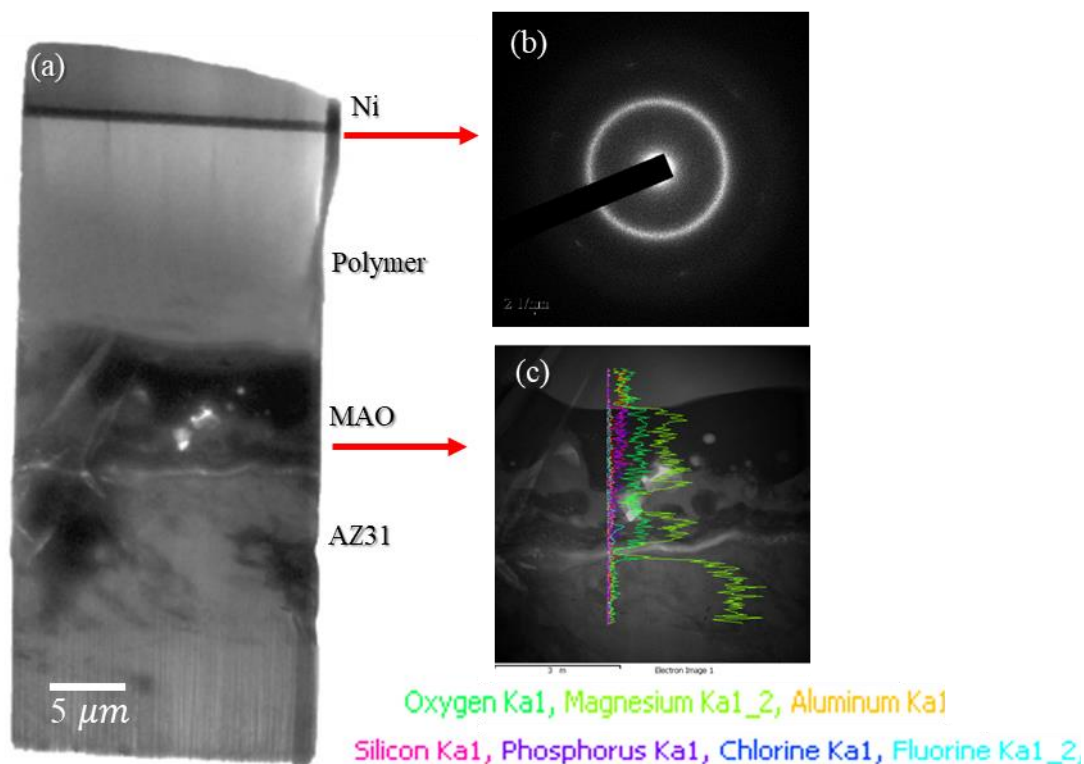
Figure 5. The TEM analysis of MAO/polymer/Ni three layers coatings: (a)TEM micrograph, (b)SAED, (c) composition line scan

The SADE image indicates the Ni film has an amorphous structure with some nano-crystalline. The chemical composition of Ni film analyzed by TEM-EDS presented that the phosphorus content of Ni film is approximately at 15.45 at% (Table 3).

The chemical composition of AZ31, MAO, polymer layer are also presented in Table 3, respectively. From Fig 5(a),(c), it can be observed that the MAO film, polymer film and Ni layer are successfully deposited on the AZ31 magnesium alloy substrates. By comparing with Fig. 2, it can be observed that there are many large size micro-arc holes in MAO film without deposited polymer layer.

From the analysis of TEM-EDS (Fig. 5(c) and Table 3), the carbon concentration is approximately at 89.64 at.% near the polymer and MAO layer, indicating the pores on the surface of the MAO are evenly sealed by polymer.

3.2. Mechanical property and corrosion behavior

Two different solutions are used to measure the contact angle including DI water and 3.5 wt% NaCl solution, the test result is shown in Fig 6. Using DI water to measure the contact angle of AZ31 magnesium alloy, MAO layer, polymer layer and Ni layer, and their contact angle is 63.7°, 60.7°, 92.4° and 84.5°, respectively. Using 3.5 wt% NaCl solution to measure the contact angle of AZ31 magnesium alloy, MAO layer, polymer layer and Ni layer, the contact angle is 58.3°, 54.2°, 107.8° and 90.0°, respectively. The result of contact angle test presents the hydrophobicity of MAO coating are

significantly improved after sealing by polymer layer. Therefore, it can effectively prevent penetration in corrosion, improve substrate protection and increase corrosion resistance. Moreover, the hydrophobicity of the coating is beneficial to prevent water droplets from sticking to the surface of the coating, and it is also beneficial to the corrosion resistance of coatings.
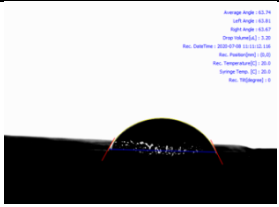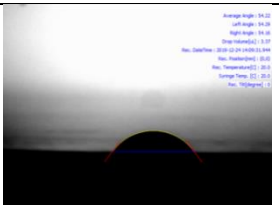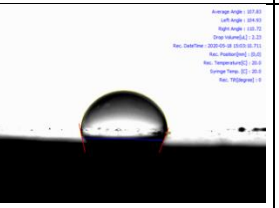
	AZ31 magnesium alloy	MAO layer	polymer layer	Ni layer
DI water				
contact angle	63.7	60.7	92.4	84.5
3 wt % NaCl solution				
contact angle	58.3	54.2	107.8	90.0

Figure 6. The contact angle analysis of AZ31 magnesium alloy, MAO layer, polymer layer and Ni layer using DI water and 3 wt % NaCl solution.
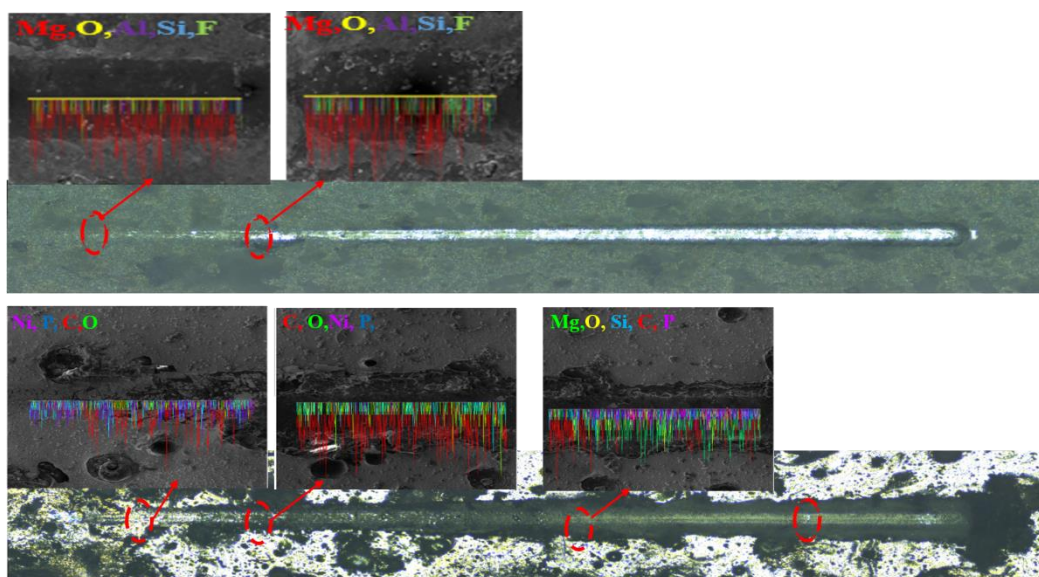

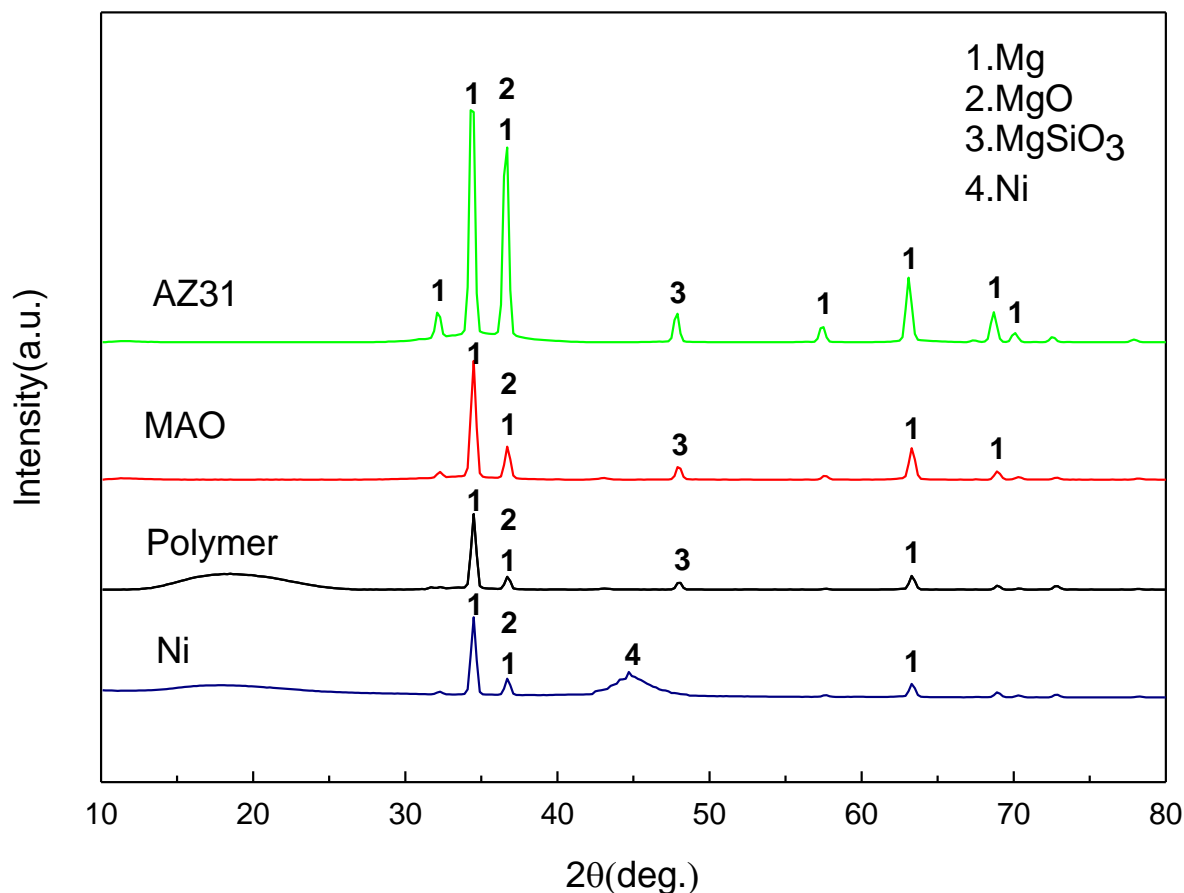**Figure 7.** The scratch test images (a) MAO layer, (b) Ni layer.

Figure 8. The XRD pattern of AZ31 magnesium alloy, MAO film, polymer film and Ni film.

The scratch test result of MAO layer and Ni layer are shown in Fig. 7. Fig 7a shows the L_{c1} of MAO layer occurs at 2.02 N, it can be judged that this is the lowest critical load. When the load increases to 4.71 N, the depth curve of the scratches changes sharply, indicating at 4.71N the coating can no longer withstand this force, resulting in deformation and lateral accumulation of the coating, so this load is the maximum critical load L_{c2}. Fig 7b shows the L_{c1} of Ni layer occurs at 2.78 N, it can be judged that this is the lowest critical load. When the load increases to 4.41 N, indicating Ni coating can no longer withstand this force. From the SEM-EDS-Mapping image, it can be seen that the carbon element has increased significantly while the nickel element has decreased, so it can be judged that the Ni layer has been cracked and scratched to the polymer film layer. When the load increases to 11.65 N, the depth curve changes.
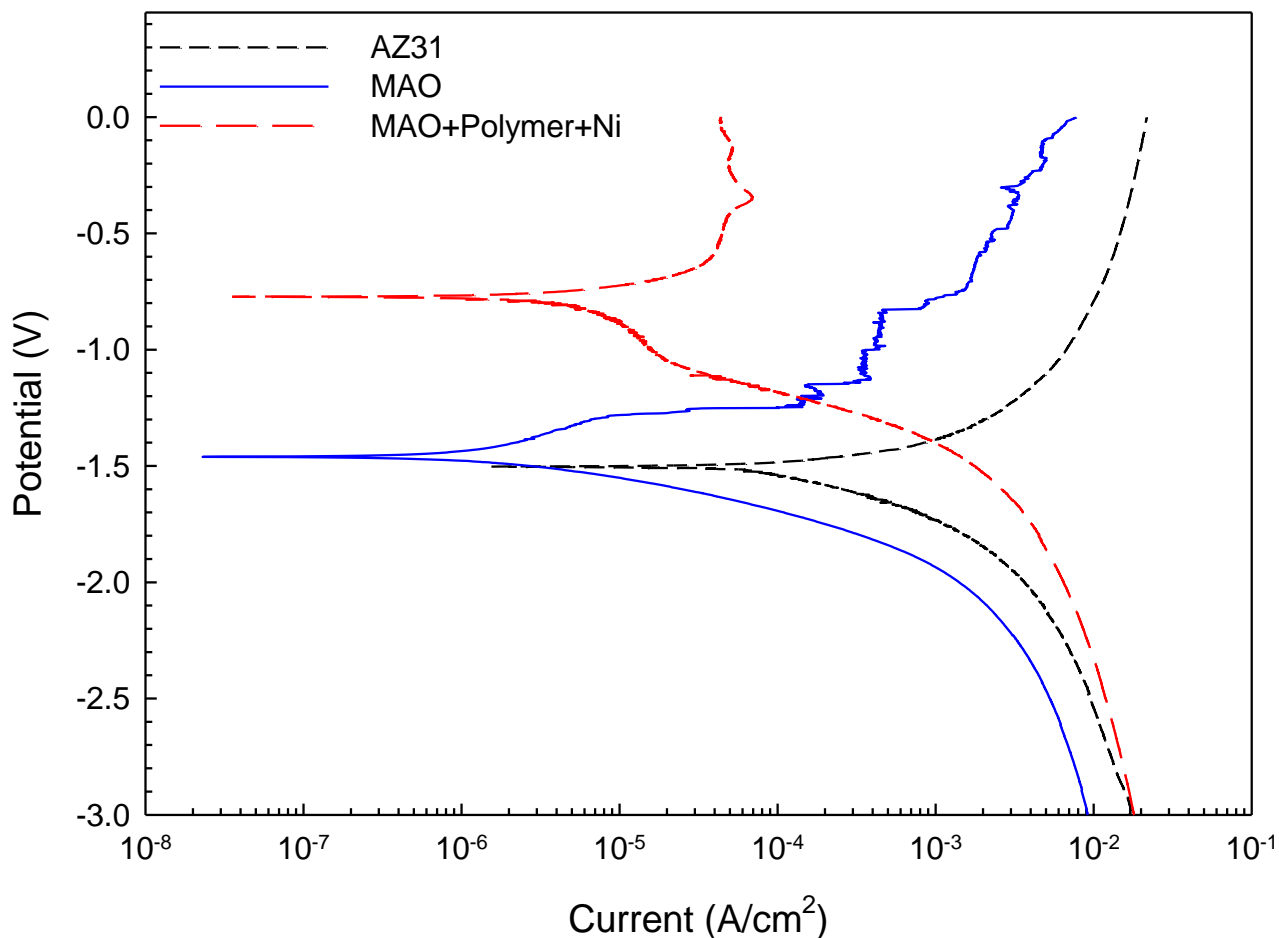
Figure 9. Potentiodynamic curves of AZ31 magnesium alloy, MAO film and MAO/polymer/Ni three layers coatings.

From the SEM-EDS-Mapping image, it can be seen that the carbon element begins to decrease and the MgO composition increases. It is judged that the polymer film can no longer withstand this force. When the load increases to 16.46N, it causes the coating to deform and laterally accumulate. It is judged that the MAO layer can no longer withstand this force, here is the maximum critical load L_{c2}.

The HR-XRD analysis of various layers, including AZ31 magnesium alloy, MAO layer, polymer layer and Ni layer are prepared as shown in Fig.8. Owing to the micro-arc oxidation electrolyte contains Na_2SiO_3, therefore, MgO, $MgSiO_3$ will be formed in the MAO layer after micro-arc oxidation. The MAO film after coating the polymer layer, the Mg, MgO and $MgSiO_3$ is still can be identified by XRD. A broaden Ni diffraction peak shows in the MAO/polymer/Ni three layers coatings, indicating the Ni layer has an amorphous structure, which also be confirmed by SADE. The average grain size of Ni film is calculated by Scherrer formula, and the grain size is approximately at 4.33 nm. Polarization curves of AZ31 magnesium alloy, MAO film and MAO/polymer/Ni three layers coatings are shown in Fig. 9 and the value of i_{corr} and E_{corr} are shown in Table 4.

Table 4. Corrosion resistance of AZ31 magnesium alloy, MAO layer and Ni layer analyzed from 3.5 wt.% NaCl solution.

	AZ31 magnesium alloy	MAO layer	MAO/polymer/Ni three layers
Current density/ A/cm^2	712 μA/cm^2	39.6 μA/cm^2	7.2 μA/cm^2
Potential/V	-1.518V	-1.453V	-0.762V

The i_{corr} of AZ31 magnesium alloy, MAO film and MAO/polymer/Ni three layers coatings is approximately at 712×10^{-6} A/cm^2, 39.6×10^{-6} A/cm^2 and 7.2×10^{-6} A/cm^2, respectively. The results show that MAO/polymer/Ni three layers coatings have the best corrosion resistance. From TEM images (Fig. 5), it can found that the microstructures of the polymer layer and Ni layer are dense and have no micro-pores, and most of the fluorine elements are deposited under the MAO film layer. However, when the MAO layer is not coated with a polymer layer, the MAO layer has more micro-arc holes and larger holes. In this study, after the polymer agent is spin-coated, the polymer coating can indeed penetrate into the pores of the MAO layer. Since the coated polymer film will seal the pores on the surface of the MAO and increase the hydrophobicity of the coating (Fig. 6), it will increase the corrosion resistance of the coating and provide effective corrosion protection for the magnesium alloy. The above experimental result is agreement with previous studies [22,23].

4. CONCLUSION

The effect of MAO/polymer/Ni three layers coatings to improve the corrosion resistance of MAO film is studied in this study. Observations from SEM and TEM showed that the microstructures of the polymer layer and Ni layer are dense and without micro-pores, and most of the fluorine elements are deposited in the bottom of MAO film layer. Via ultrasound and Spin coating can indeed allow the polymer agent to effectively penetrate into the MAO pores and seal the surface pores of the MAO layer to increase its hydrophobicity, thereby increasing its corrosion resistance. The value of i_{corr} of MAO/polymer/Ni three layers is 7.2×10^{-6} A/cm^2, significantly better than that of MAO film is 39.6×10^{-6} A/cm^2. The result of scratch test show that the adhesion of MAO/polymer/Ni three layers is significantly better than that of MAO layer.

Int. J. Electrochem. Sci., 16 **(2021)** Article Number: 211246

14

References

1. J. W. Lee, H. S. Han, K. J. Han, J. Park, H. Jeon, D. Mantovani, *Proc. Natl. Acad. Sci.*, 113 (2016) 716.
2. Y. W. Song, D. Y. Shan, E. H. Han, *Electrochim. Acta*, 53 (2008) 2135.
3. P. Bala Srinivasan, J. Liang, C. Blawert, M. Störmer, W. Dietzel, *Appl. Surf. Sci.*, 255 (2009) 4212.
4. B. Bozzoni, C. Lenardi, M. Serra, M. Faniglulio, *Br. corros. j.*, 37 (2002)173.
5. X. Lei, T. Liu, J. Chen, B. Miao, W. Zeng, Materials Transactions, 52 (2011) 1082.
6. J. T. Yao , Sheng Wang , Yong Zhou, Hui Dong, *Metals*, 10 (2020) 1452.
7. R. Kamal Jayaraj, S. Malarvizhi, V. Balasubramanian, *Def. Technol.*, 13 (2017) 111.
8. Y. Pan, K. Wang, D. G. Chen, *Mater. Lett.*, 119 (2014) 127.
9. G. Wu, D. Zhao, X. Lin, J. Liu, X. Ji, *Surf. Interfaces*, 20 (2020) 100513.
10. J. Zhang, Y. Fan, X. Zhao, R. Ma, X. Du, A. Cao, *Surf. Coat. Technol.*, 337 (2018) 141.
11. P. Wang, T. Wu, Y. Xiao, T. Zhang, L. Pu, J., Cao, W. J. Zhong, X. M, *Vacuum*, 142 (2017) 21.
12. M. Kaseem, T. Hussain, Z. Rehman, U.G.Y. Ko, *J. Alloys Compd.*, 853 (2021) 157036.
13. X. Yang, W. L. Wang, W. J. Ma, Y. Wang, S. F. Liu, *Transactions of Nonferrous Metals Society of China*, 30 (2020) 2132.
14. A.L. Yerokhin, A.Shatrov, V. Samsonov, P. Shashkov, A. Leyland, A. Matthews, *Surf. Coat. Technol.*, 182 (2004) 78-84.
15. Y. Chen, S. Zhao, B. Liu, M. Chen, J. Mao, *ACS Appl. Mater. Interfaces*, 6 (2014) 19531.
16. X. Zhan, W. Shang, Y. Wen, Y. Li, M. Ma, *J. Alloys Compd.*, 774 (2019) 522.
17. G. B. Darband, M. Aliofkhazraei, P. Hamghalam, N. Valizade, *J. Magnes. Alloy.*, 5 (2017) 74-132.
18. V. Ezhilselvi, J. Nithin, J. N. Balaraju, S.Subramanian, *Surf. Coat. Technol.*, 288 (2016) 221.
19. F. Bentiss, M. Traisnel & M. Lagrenee, *J. Appl. Electrochem.*, 31 (2001) 41.
20. H. Wei, Y. Wang, J. Guo, N. Z. Shen, D. Jiang, X. Zhang, Z. Guo, *J. Mater. Chem. A*, 3 (2015) 469.
21. H. Zhang, J. Yang, B. Chen, C. Liu, M. Zhang, C.& Li, *Appl. Surf. Sci.*, 359 (2015) 905.
22. K.A. Zahidah, S. Kakooei, M.C. Ismail, P.B. Raja, *Prog. Org. Coat.*, 111 (2017) 175.
23. F. Liu, D. Shan, Y. Song, E. H. Han, *Surf. Coat. Technol.*, 206 (2011) 455.
24. Z. Li, Q. Yu, C. Zhang, Y. Liu, J. Liang, D. Wang, F. Zhou, *Surf. Coat. Technol.*, 357 (2019) 515.
25. M. Uysal, H. Akbulut, M. Tokur, H. Algül, T. Çetinkaya, *J. Alloys Compd.*, 654 (2016) 185.
26. M. Gholizadeh-Gheshlaghi, D. Seifzadeh, P. Shoghi, A. Habibi-Yangjeh, *J. Alloys Compd.*, 769 (2018) 149.
27. R. Ambat, N. N. Aung, W. Zhou, *Corros. Sci.*, 42 (2000) 1433.
28. X. B. Chen, A. Easton, N. Birbilis, H. Y. Yang, T. B. Abbott, Woodhead Publishing, (2013) 315.
29. C. A. León-Patiño, J. García-Guerra, E. A. Aguilar-Reyes, *Wear*, 426 (2019) 330.
30. Z. C. Wang, F. Jia, L. Yu, Z. B. Qi, Y. Tang, G. L. Song, *Surf. Coat. Technol.*, 206 (2012) 3676.
31. B. Hu, R. Sun, G. Yu, L. Liu, Z. Xie, X. He, X. Zhang, *Surf. Coat. Technol.*, 228 (2013) 84.
32. M. A. Chen, N. Cheng, Y. Ou, C., J. M. Li, *Surf. Coat. Technol.*, 232 (2013) 726.
33. Z. Song, Z. Xie, G. Yu, B. Hu, X. He, X. Zhang, *J. Alloys Compd.*, 623 (2015) 274.
34. C.S. Lin, C.Y. Lee, F.J. Chen, C.T. Chien, P.L. Lin, and W.C. Chung, *J. Electrochem. Soc.*, 153 (2006) C387.
35. G. Lu, G. Z Angari, *Electrochim. Acta*, 47 (2002) 2969.